
Noise2Recon: A Semi-Supervised Framework for Joint MRI Reconstruction and Denoising

Arjun D Desai^{*1} Batu M Ozturkler^{*1} Christopher M Sandino¹ Shreyas Vasanawala¹ Brian A Hargreaves¹
Christopher M Ré¹ John M Pauly¹ Akshay S Chaudhari¹

Abstract

Deep learning (DL) has shown promise for faster, high quality accelerated MRI reconstruction. However, standard supervised DL methods depend on extensive amounts of fully-sampled ground-truth data and are sensitive to out-of-distribution (OOD) shifts, in particular for low signal-to-noise ratio (SNR) acquisitions. To alleviate this challenge, we propose a semi-supervised, consistency-based framework (termed Noise2Recon) for joint MR reconstruction and denoising. Our method enables the usage of a limited number of fully-sampled and a large number of undersampled-only scans. We compare our method to augmentation-based supervised techniques and fine-tuned denoisers. Results demonstrate that even with minimal ground-truth data, Noise2Recon (1) achieves high performance on in-distribution (low-noise) scans and (2) improves generalizability to OOD, noisy scans.

1. Introduction

Magnetic resonance imaging (MRI) is a non-invasive imaging modality with high diagnostic quality owing to its superior soft-tissue contrast. However, MRI suffers from long scan times, requiring accelerated imaging methods to enable clinical applications where rapid imaging is necessary. Parallel imaging is a commonly used method for accelerated imaging where sensitivity maps of receiver coils are utilized to resolve coherent aliasing artifacts from uniformly undersampled data (Pruessmann et al., 1999). Another powerful tool to accelerate MRI acquisition using undersampled k-space data is compressed sensing (CS), which exploits the sparsity of the reconstructed image in a hand-crafted transform domain (Lustig et al., 2008). However, these methods either have limited efficacy at large acceleration

factors or have long reconstruction times and require careful fine-tuning of hyperparameters.

Deep-learning (DL) methods have shown potential for enabling higher acceleration factors than PI and CS methods and for improving the quality of the reconstructed images (Hammernik et al., 2018; Sandino et al., 2020). The success of these methods can be attributed to their ability to capture complex image features to effectively regularize the MRI reconstruction problem and provide much faster reconstruction times compared to CS.

Despite the success of DL-based methods in MRI reconstruction, several challenges remain for widespread clinical deployment of these methods. One shortcoming of these methods is their dependence on large amounts of fully-sampled training data, which might be intractable to acquire for many applications such as dynamic-contrast-enhanced (DCE) imaging or volumetric time-resolved blood-flow imaging (4D-flow). Therefore, it is often difficult to curate large training datasets for supervised learning that solely consist of fully-sampled MR images. In such scenarios where fully-sampled images are scarce, techniques that can leverage information from more ubiquitous undersampled datasets are desirable.

Another critical shortcoming of both DL and CS-based MRI reconstruction is the limited robustness of these methods to perturbations at inference time (Chaudhari et al., 2021). Previous work has shown that small structural perturbations can result in amplified artifacts in the reconstructed images among DL and CS-based methods (Darestani et al., 2021; Lustig et al., 2007). One such perturbation that current reconstruction algorithms are vulnerable to is noise. Given the heterogeneity of MR hardware and sequence configurations, the noise level can vary considerably among different scans. For iterative CS methods, the maximum rate of undersampling for reasonable signal recovery is bounded by measurement noise (Donoho et al., 2011). As a consequence, CS-based MRI reconstructions might fail to converge to a feasible solution in high noise regimes (Virtue & Lustig, 2017). The reconstruction quality of DL-based methods also degrades considerably when a deviation in SNR between training and testing is present (Knoll et al., 2019). There-

^{*}Equal contribution ¹Stanford University. Correspondence to: Arjun D Desai <arjundd@stanford.edu>, Batu M Ozturkler <ozt@stanford.edu>.

Preprint.

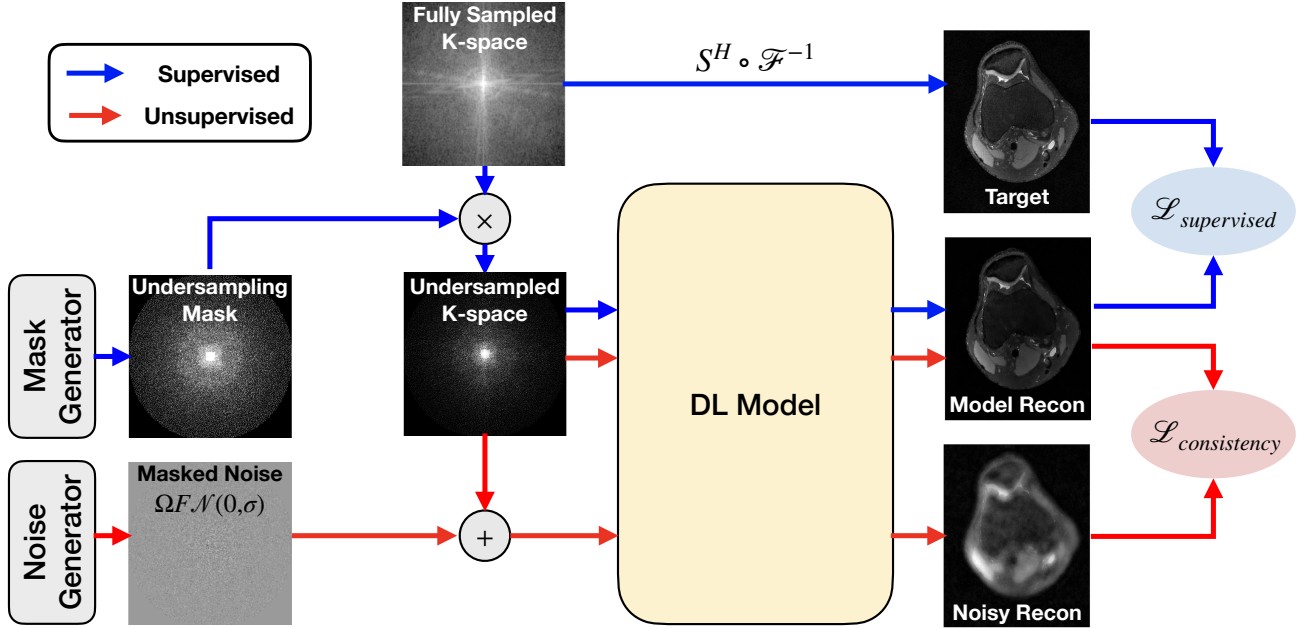


Figure 1. The Noise2Recon schematic for semi-supervised joint reconstruction and denoising. Fully-sampled scans follow the supervised training paradigm (blue arrows). Undersampled scans are augmented with zero-mean complex Gaussian noise with standard deviation σ , which is sampled from a predefined range. The model reconstructs both the non-augmented and augmented scans. The reconstruction of the non-augmented scan is used as a pseudo-label for the reconstruction of the augmented scan, a process which we refer to as *consistency*. The total loss is a weighted sum of the supervised and consistency losses: $\mathcal{L}_{total} = \mathcal{L}_{supervised} + \lambda\mathcal{L}_{consistency}$.

fore, it is crucial to develop reconstruction networks that are robust to noise in sensitive applications such as accelerated MRI reconstruction.

Motivated by these challenges, we propose Noise2Recon (N2R), a semi-supervised DL framework that performs joint MRI reconstruction and denoising. In Noise2Recon, available fully-sampled reference scans are used to train a model with respect to a supervised MRI reconstruction objective. For each scan without a fully-sampled reference, Noise2Recon generates reconstructions for both the undersampled scan and a noise-augmented rendition of the scan. A consistency loss is used between the clean and noisy reconstructions to enforce the model to be robust to noise that is present in the forward model of the imaging system. A schematic of our method is shown in Figure 1. At its core, Noise2Recon’s consistency-based framework utilizes *both* fully-sampled and undersampled scans to enable reconstruction in data-limited settings and to increase robustness to noise.

The main contributions of this work can be summarized as follows:

1. We propose a semi-supervised method for joint MRI reconstruction and denoising using consistency-based training via noise augmentations.

2. We demonstrate our method outperforms state-of-the-art CS and DL baselines in data-limited settings.
3. We show our method increases robustness for recovering images in out-of-distribution, noisy acquisitions.

2. Related Work

In this section, we outline existing supervised image reconstruction methods as well as data-limited image reconstruction and image denoising methods that motivated our proposed method.

2.1. Supervised Image Reconstruction

The vast majority of image recovery methods perform learning in a supervised fashion, where a large dataset consisting of fully-sampled references is needed to perform training. One of the common approaches in supervised learning is to directly invert the forward imaging model using a feed-forward convolutional neural network (CNN) architecture (Zhang et al., 2017; Jin et al., 2017). An alternative to direct inversion is to unroll an iterative algorithm for a fixed number of iterations and alternate between a data-fidelity term and a regularization term, where the regularization function is learned in a data-driven fashion (Pezzotti et al., 2020; Adler & Öktem, 2018; Meinhardt et al., 2017; Aggarwal

et al., 2019). However, these methods require large number of fully-sampled scans and are not designed to leverage undersampled scans.

2.2. Data-Limited Image Reconstruction

To tackle this supervised data-dependence problem, data-limited image reconstruction has gained popularity, where methods mainly differ by the imposed imaging prior, the proposed network architecture, or the use of data augmentation. Generative adversarial networks have been proposed for data-limited reconstruction using unpaired datasets (Lei et al., 2021) or only undersampled datasets (Cole et al., 2020). (Liu et al., 2020) extends regularization by denoising (RED) (Romano et al., 2017) to utilize priors from more general artifact removal networks, whereas (Darestani & Heckel, 2021) use untrained networks to incorporate the prior of the architecture of a convolutional neural network (CNN). Other methods involve self-supervised learning (Yaman et al., 2020) and dictionary-based learning (Lahiri et al., 2021) to enable data-limited reconstruction. Recently, image-based augmentations were also verified to help decrease data dependence for fully-supervised networks (Fabian et al., 2021). While these approaches reduce dependence on fully-sampled data, they do not provide a clear framework for leveraging both fully-sampled and undersampled scans for semi-supervised model training. In addition, these methods can be brittle under distribution shift induced by common perturbations (e.g. noise) (Knoll et al., 2019; Darestani et al., 2021).

2.3. Data-Limited Image Denoising

More recently, there have been many approaches proposed for image denoising problems that do not require access to a large dataset with fully-sampled references. Before DL approaches, plug-and-play priors (Venkatakrishnan et al., 2013), as well as the iterative application of image denoisers as imaging priors via RED (Romano et al., 2017) were shown to be very effective in a wide range of inverse problems. Later, (Lehtinen et al., 2018) showed that image recovery with neural networks can be performed without ground-truth images by only using images corrupted by zero-mean noise.

Extensions of this idea have also been proposed where a network is trained via self-supervision using only noisy images to model denoising (Batson & Royer, 2019; Hu & Cheng, 2021) and the imaging inverse problem at hand (Hendriksen et al., 2020). However, these methods operate under the assumption that noise exhibits statistical independence across different dimensions of the measurements. In addition, in the Gaussian noise setting, Stein’s unbiased risk estimator can be used as a surrogate for minimizing mean-squared-error to perform denoising using only noisy images

(Soltanayev & Chun, 2021).

Our method is a semi-supervised learning approach where a supervised loss is combined with an unsupervised consistency loss, with the aim of leveraging undersampled datasets. Consistency training acts as a regularizer to improve robustness to noise-augmented input examples, and was shown to be effective for semi-supervised natural image classification when a large unlabeled dataset is available in addition to a small labeled dataset (Sohn et al., 2020; Xie et al., 2020). The advantage of the consistency-training-based formulation is that no assumptions are required on the statistical properties of the input signal to reconstruct in contrast to aforementioned image denoising approaches.

3. Methods

In this section, we first introduce the operating notation for the reconstruction problem. We then formalize the optimization for supervised MR reconstruction training and for self-supervised denoising training. Finally, we introduce our proposed semi-supervised framework for joint MR reconstruction and denoising from limited labeled data.

3.1. Notation

We consider the multi-coil accelerated MR acquisition setup, where the observed k-space samples are acquired across multiple receiver coils. The forward model for this problem can be formulated as follows:

$$y = \Omega F S x^* + \epsilon \tag{1}$$

where y is the set of observed, complex-valued measurements in k-space for all coils, x^* is the true image we would like to reconstruct, S is the set of sensitivity maps associated with each receiver coil, F is the Fourier transform matrix, and Ω is the k-space undersampling mask. ϵ is the *masked* additive complex Gaussian noise resulting from thermal noise (Macovski, 1996). ϵ is the same dimension as y .

Consider a dataset \mathcal{D} that consists of scans with fully-sampled (supervised) k-space data ($\mathcal{D}^{(s)}$) and scans with only undersampled (unsupervised) k-space data ($\mathcal{D}^{(u)}$). Dataset \mathcal{D} is then the union of the two sets of scans ($\mathcal{D} = \mathcal{D}^{(s)} \cup \mathcal{D}^{(u)}$). Additionally, scans are either fully-sampled or undersampled, but not both. Thus, there is no overlap between fully-sampled scans and undersampled scans (i.e. $\mathcal{D}^{(s)} \cap \mathcal{D}^{(u)} = \emptyset$). $y_i^{(s)} \in \mathcal{D}^{(s)}$ and $y_j^{(u)} \in \mathcal{D}^{(u)}$ are the k-space measurements of the i^{th} example in the supervised dataset and j^{th} example in the unsupervised dataset, respectively. $x_i^{(s)}$ is the image space counterpart of $y_i^{(s)}$. f_θ is the model parameterized by θ trained to reconstruct images from undersampled data. The operator $|\cdot|$ denotes the cardinality. In practice, $|\mathcal{D}^{(s)}| \ll |\mathcal{D}^{(u)}|$.

3.2. Supervised MRI Reconstruction

In supervised MRI reconstruction, training is performed using only data where fully-sampled references exist (i.e. $\mathcal{D}^{(s)}$). In these cases, an undersampled input can be simulated by sampling an undersampling mask Ω from a distribution of undersampling patterns Ω and applying these masks to the fully-sampled k-space $y_i^{(s)}$. As fully-sampled scans are retrospectively undersampled, different masks can be generated for different inputs. End-to-end training of model f_θ minimizes

$$\min_{\theta} \frac{1}{|\mathcal{D}^{(s)}|} \sum_i \mathcal{L}_{sup}(f_\theta(\Omega y_i^{(s)}), x_i^{(s)}) \quad (2)$$

where \mathcal{L}_{sup} is a supervised loss function, and f_θ includes the mapping that transforms k-space to image-space.

To avoid overfitting in data-scarce settings, supervised reconstruction methods can use data augmentation to simulate larger labeled training datasets (Fabian et al., 2021). For simplicity, we consider a single label-invariant augmentation. Formally, the loss for example $x_i^{(s)}$ is written as

$$\mathcal{L}_{sup}(f_\theta(T_p(\Omega y_i^{(s)})), x_i^{(s)}) \quad (3)$$

where transform T is applied to the input with probability p and supervised with respect to the original input.

3.3. Unsupervised Image Denoising

Unsupervised denoising techniques can be formulated by selecting an example x_i , corrupting the example with a known or expected signal corruption model Ψ , and training a model to recover the original signal x_i from the corrupted signal $\Psi(x_i)$. More formally this can be written as

$$\min_{\theta} \mathbb{E}[\mathcal{L}(f_\theta(\Psi(x_i)), x_i)] \quad (4)$$

where \mathcal{L} is an arbitrary regression loss function that is often chosen to be the ℓ_1 loss (Zhao et al., 2016). When calculated over complex images, ℓ_1 loss corresponds to the absolute value of the complex loss, defined by its Euclidean norm.

In the denoising problem,

$$\Psi(x) = x + \epsilon \quad (5)$$

where ϵ is the noise drawn from a predefined distribution \mathcal{N} . Note that the corruption model does not make the assumption that the input has a reference label. As a result, both data with and without ground-truth references can be used as a target for the model. Additionally, let \tilde{x}_i be the low-quality counterpart of x_i which is high-quality, i.e. \tilde{x}_i is sampled from a corrupted distribution. If the assumption

$\mathbb{E}\{\tilde{x}_i | \Psi(x_i)\} = x_i$ holds, Eq. 4 is equivalent to the training problem in (Lehtinen et al., 2018). This assumption is valid in the case of zero-mean noise and is necessary for predicting unbiased estimates of $\Psi(x_i)$.

3.4. Proposed Method: Noise2Recon

Current supervised reconstruction methods achieve state-of-the-art results with large amounts of fully-sampled data, but these methods are prone to overfitting in data-scarce settings. Model regularization techniques, such as ℓ_1/ℓ_2 regularization, can help mitigate overfitting; however, these methods are based predominantly on prior-driven assumptions about model weights (e.g. sparsity). Given that fully-sampled data can often be scarce, reconstruction methods that can leverage a mixture of fully-sampled and prospectively undersampled data and incorporated data-driven regularization would be helpful. Additionally, while both denoising and reconstruction tasks are critical for recovering high quality images, they are formulated as disjoint, sequential operations. The separation of these objectives may be optimal for each task individually, but may lead to poor optimization for both tasks jointly.

In this work, we propose a semi-supervised framework for joint MR reconstruction and denoising that mitigates overfitting in data-scarce settings and increases robustness to noisy OOD acquisitions. Noise2Recon complements the supervised training paradigm described in §3.2 by adding a noise-augmentation consistency training paradigm (Fig.1). Examples without fully-sampled references (unsupervised) are augmented with masked additive noise. The model f_θ generates reconstructions for both unsupervised images ($f_\theta(y^{(u)})$) and noise-augmented unsupervised images ($f_\theta(y^{(u)} + \Omega_{y^{(u)}}\epsilon)$), where $\Omega_{y^{(u)}}$ is the undersampling mask that was used to acquire unsupervised example $y^{(u)}$. A consistency loss (\mathcal{L}_{cons}) is enforced between reconstructions of the unsupervised examples and their noise-augmented counterparts to build noise-invariant reconstruction models. End-to-end training with Noise2Recon seeks to minimize a weighted sum of the supervised loss (\mathcal{L}_{sup}) and the unsupervised consistency loss (\mathcal{L}_{cons}). Thus, the objective can be written as

$$\min_{\theta} \mathbb{E}[\mathcal{L}_{sup}(f_\theta(\Omega y^{(s)}), x^{(s)})] + \lambda \mathbb{E}[\mathcal{L}_{cons}(f_\theta(y^{(u)} + \epsilon), f_\theta(y^{(u)}))]$$

where undersampling mask Ω can be randomly generated for fully-sampled data, λ is a weighting constant, and ϵ is a randomly generated masked noise map.

Simulating noise for consistency augmentations:

Noise in MRI is dominated by thermal fluctuations in the subject and, to some extent, the receiver electronics. This noise source can be modeled as additive

Acceleration (R)	Method	SSIM	nRMSE	pSNR (dB)
12x	Compressed Sensing	0.846 (0.012)	0.175 (0.012)	37.29 (0.32)
	Supervised	0.827 (0.031)	0.162 (0.007)	37.96 (0.24)
	Supervised (FT)	0.810 (0.036)	0.157 (0.015)	38.24 (0.64)
	Supervised + Aug	0.816 (0.035)	0.163 (0.008)	37.86 (0.28)
	Supervised + Aug (FT)	0.810 (0.037)	0.157 (0.015)	38.23 (0.69)
	Noise2Recon (Ours)	0.901 (0.018)	0.142 (0.013)	39.08 (0.63)
16x	Compressed Sensing	0.847 (0.011)	0.178 (0.013)	37.12 (0.35)
	Supervised	0.810 (0.032)	0.171 (0.009)	37.49 (0.23)
	Supervised (FT)	0.809 (0.037)	0.160 (0.014)	38.04 (0.61)
	Supervised + Aug	0.812 (0.042)	0.172 (0.009)	37.41 (0.27)
	Supervised + Aug (FT)	0.787 (0.039)	0.167 (0.012)	37.69 (0.48)
	Noise2Recon (Ours)	0.887 (0.018)	0.151 (0.012)	38.58 (0.47)

Table 1. Average performance of different reconstruction methods trained with 1 supervised scan ($k = 1$) and 13 unsupervised scans. Fine-tuned networks (FT) were first pretrained with the denoising task on both supervised and unsupervised data and subsequently fine-tuned for reconstruction on 1 supervised scan. Compressed sensing used l1-wavelet regularization ($\lambda=0.07$ (12x), 0.06 (16x)). Metrics are reported as *mean (standard deviation)*.

complex-valued Gaussian noise added to each acquired k -space sample (Macovski, 1996). Thus, for unsupervised example $y_i^{(u)}$, we generate masked complex-gaussian noise $\epsilon_i \sim \Omega_{y_i^{(u)}} \mathcal{FN}(0, \sigma_{tr})$, where \mathcal{N} is a zero-mean complex-gaussian distribution with standard deviation σ_{tr} , which is chosen from a specified range $\mathcal{R}(\sigma_{tr}) = [\sigma_{tr}^L, \sigma_{tr}^U]$. σ_{tr} is normalized with respect to the magnitude of the image such that it induces the same relative change in SNR across scans.

Balanced data sampling: As the supervised and consistency objectives are computed over a disjoint set of examples, the weighting of each objective is governed, in expectation, by the rate of sampling from $\mathcal{D}^{(s)}$ and $\mathcal{D}^{(u)}$, respectively. More formally,

$$\mathbb{E}\left[\frac{\nabla_{\theta}\mathcal{L}_{cons}}{\nabla_{\theta}\mathcal{L}_{sup}}\right] \propto \frac{|\mathcal{D}^{(u)}|}{|\mathcal{D}^{(s)}|}. \quad (6)$$

In this setting, the optimization is sensitive to the ratio of supervised to unsupervised examples. One solution to this would involve modifying λ for different relative dataset sizes. However, this solution would require extensive tuning for λ and would still perpetuate uneven optimization at different stages of the training cycle.

We propose a balanced data sampling scheme that samples unsupervised and supervised examples at a rate determined by a fixed ratio $T_S:T_U$. For every T_S supervised examples that are sampled during training, T_U unsupervised examples are sampled. In this formulation, this sampling method implicitly eliminates the influence of the relative sizes of the supervised and unsupervised datasets on the relative

weighting between the supervised and consistency objectives.

4. Experiments

Our goal is to demonstrate that Noise2Recon can leverage noise augmentations for task-based regularization that can improve performance in both high- and low-SNR settings. We show that Noise2Recon can (1) outperform standard supervised methods in data-scarce scenarios and (2) improve robustness to reconstruction in noisy settings. We conduct extensive ablations to isolate the advantages of the consistency objective and the balanced sampling.

4.1. Dataset

We performed experiments on the publicly available fully-sampled 3D fast-spin echo (FSE) multi-coil knee scans (acquisition matrix $k_x \times k_y \times k_z=320 \times 320 \times 256$) from mri-data.org (Ong et al., 2018). The dataset of 19 subjects was partitioned into 14 subjects (4480 slices) for training, 2 subjects (640 slices) for validation, and 3 subjects for testing. Sensitivity maps for each volume were estimated using JSENSE (implemented in SigPy (Ong & Lustig, 2019)) with a kernel-width of 8 and a 20×20 center k -space auto-calibration region (Ying & Sheng, 2007). Fully-sampled data were retrospectively undersampled with a 2D Poisson Disc undersampling pattern with the same auto-calibration region. For testing, a unique, deterministic undersampling trajectory was generated for each testing volume using a fixed random seed for reproducibility.

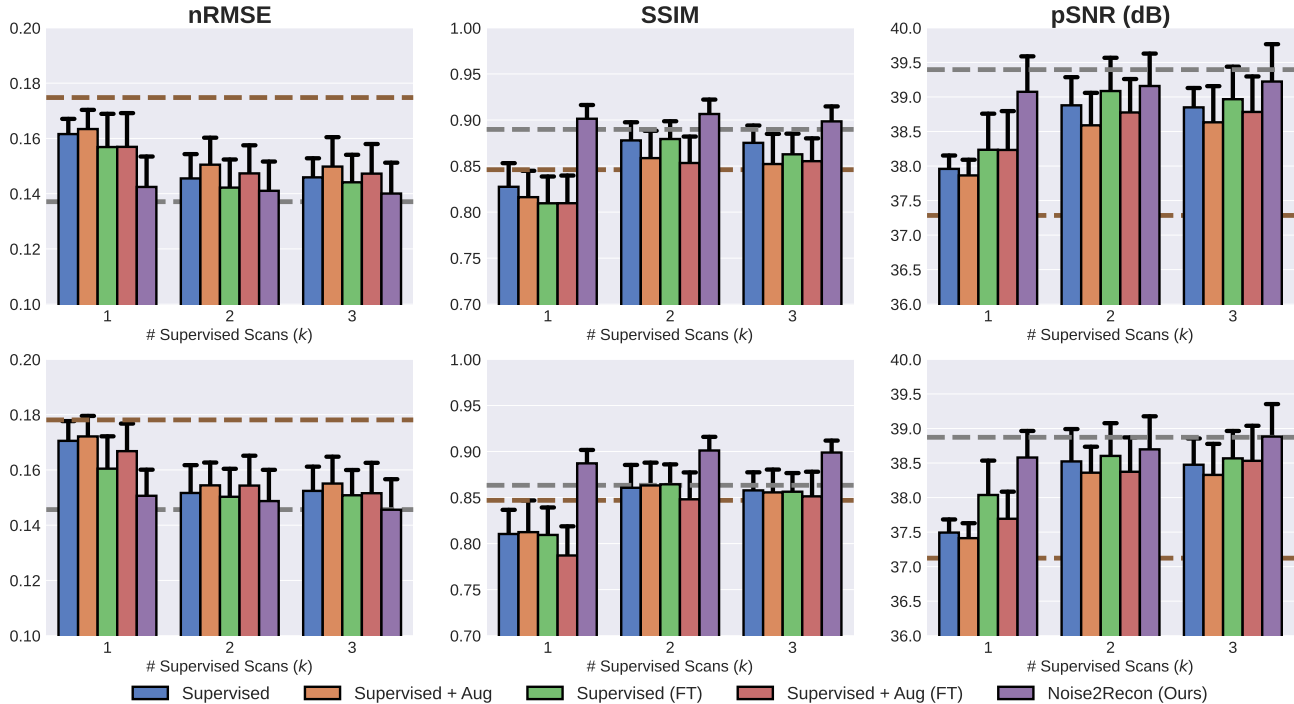


Figure 2. Reconstruction performance in label scarce settings ($k = 1, 2, 3$) at accelerations of 12x (top) and 16x (bottom). With only one supervised scan, Noise2Recon outperformed supervised methods and clinical compressed sensing baselines (brown dashed line) and approached performance of the Supervised baseline trained with $k=14$ scans (gray dashed line).

4.2. Implementation Details

3D scans were demodulated and decoded using the 1D orthogonal inverse Fourier transform along the readout direction, resulting in a hybrid k-space of dimensions $x \times k_y \times k_z$. 2D $k_y \times k_z$ slices were reconstructed by using the baseline approaches and our method.

All deep-learning approaches were trained end-to-end using the U-Net architecture implemented in the fastMRI challenge (Muckley et al., 2020; Ronneberger et al., 2015) and the complex- ℓ_1 objective (see Appendix A.1 for architecture details). Models were trained on zero-filled, SENSE-reconstructed complex images generated using the estimated sensitivity maps described in §4.1. Complex images were represented with two-channels, which corresponded to the real and imaginary components, respectively. Inputs were normalized by the 95th-percentile of the image magnitude. To preserve the magnitude distribution during metric computation at inference, outputs of the model were scaled by the normalizing constant.

We report results on three common image quality metrics computed on magnitude images: peak signal-to-noise ratio (PSNR, dB), normalized root-mean-square error (nRMSE), and structural similarity (SSIM) (Wang et al., 2004).

4.3. Simulations

Label scarcity: To evaluate the performance of different methods in label-scarce settings, scans in the training dataset \mathcal{D} were further subsampled. Fully-sampled references were dropped for $|\mathcal{D}| - k$ scans in training dataset, where k is the number of fully-sampled scans to retain. More formally, $\mathcal{D}_k \subset \mathcal{D}$ is the set of k training scans for which fully-sampled references are available. A fixed undersampling mask was generated for each scan not in \mathcal{D}_k (i.e. $x \in \mathcal{D} \setminus \mathcal{D}_k$) to simulate undersampled, reference-less scans. The extent of label scarcity was simulated with different values of k such that larger subsets are supersets of smaller subsets - i.e. $\mathcal{D}_1 \subset \mathcal{D}_2 \cdots \subset \mathcal{D}_N$.

Noisy data: Noisy acquisitions were simulated for testing scans to characterize how different methods generalize to reconstructing noisy OOD scans. For a given noise level σ_{test} , an uncorrelated multi-channel masked zero-mean complex-Gaussian noise map was generated and added to the undersampled measurements from each coil. The coil measurements were first scaled by the 95th percentile of the magnitude image such that the addition of the noise map would result in an equal reduction of SNR among all scans. Noise level σ_{test} was varied from 0, 0.1, ..., 1.0. Sample zero-filled SENSE-reconstructed images at different noise levels are shown in Figure 12 in Appendix C.

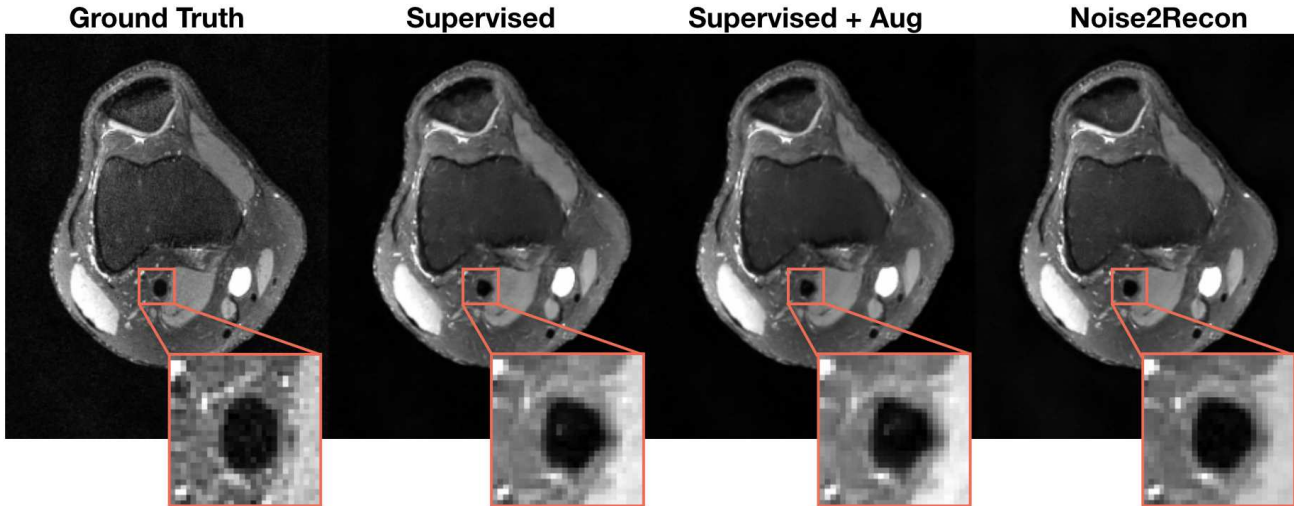


Figure 3. Sample images at 12x acceleration from supervised training methods. In data-limited settings, Noise2Recon improves performance over supervised baselines by utilizing information from unsupervised scans through consistency regularization, resulting in high-fidelity image reconstruction. Noise2Recon preserves the shape of anatomies such as the popliteal artery, as shown in the inset image.

4.4. Baseline Methods

Supervised training: Supervised models were trained both without and with noise augmentations. Augmentations were designed to be equivalent to those used in comparable Noise2Recon configurations and were applied with a probability of $p=0.2$ (see Appendix B.2 for hyperparameter details). All models were trained with only the available fully-sampled scans in the training dataset.

Fine-tuning from denoisers: Given the prior work indicating the generalizability of pretrained denoisers, we evaluated the efficacy of fine-tuning denoisers for the reconstruction task. For comparison, number of training steps was split evenly between denoising pretraining and reconstruction fine-tuning. Training and configuration setups are detailed in Appendix A.2.

Compressed sensing (CS): We included compressed sensing with l1-wavelet regularization (Lustig et al., 2007), a clinically used scan-specific, iterative reconstruction method, as an additional baseline. Reconstruction was performed slice-by-slice using SigPy where the proximal gradient method was run for 25 iterations (Ong & Lustig, 2019). Details on selection of the regularization parameter λ is provided in A.3.

5. Results

5.1. Baseline Comparisons

In these experiments, we evaluate how Noise2Recon performed compared to supervised DL and CS baselines in (1)

label scarce settings, where only a subset of training scans have ground-truth references, and (2) OOD settings, such as low-SNR acquisitions and unseen accelerations.

Label scarce settings: Noise2Recon outperformed both DL and CS baselines in label-scarce settings. Table 1 shows the average performance of different methods trained with 1 supervised scan ($k=1$). With *14 times fewer* supervised training examples, Noise2Recon performs on par with supervised methods (Fig. 2). In addition, Noise2Recon performance did not drop as the number of supervised scans increased. Qualitatively, reconstructions with Noise2Recon had considerably less blurring and reduced noise around key anatomical structures than DL baselines trained with the same number of supervised scans (Fig. 3).

Reconstructing low SNR data: Among data-driven methods, those that used noise-based augmentations (i.e. Noise2Recon, Supervised+Aug, and Supervised+Aug-FT) achieved higher image quality compared to their non-augmented counterparts (Supervised and Supervised-FT), which amplified noise artifacts at higher noise levels (Fig. 4). Unlike the augmentation-based approaches, Supervised and Supervised-FT performance also deteriorated with increase in training data. While the metrics for Supervised+Aug and Supervised+Aug-FT methods were higher than non-augmentation approaches, images reconstructed with these methods were considerably blurrier than the reconstructed images from non-augmentation baselines. In contrast, Noise2Recon sufficiently suppressed noise artifacts without excessively blurring the image (Fig. 5). On the

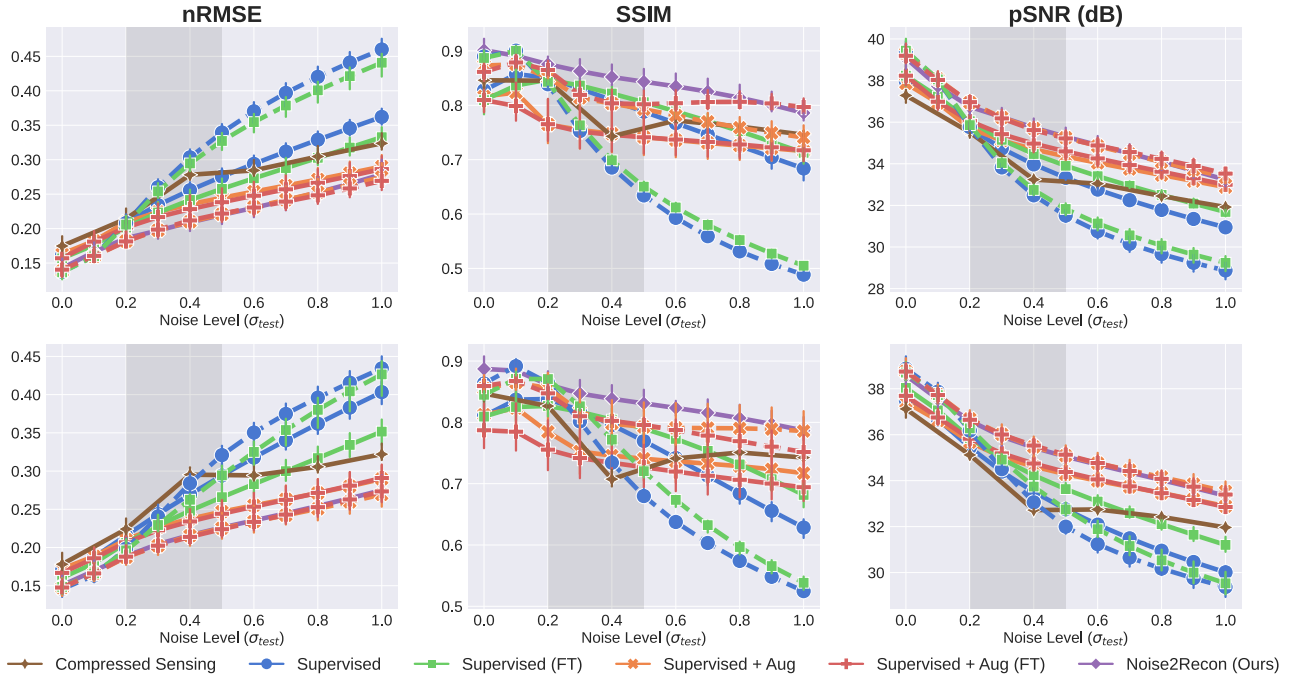


Figure 4. Characterizing reconstruction performance at varying noise levels ($\sigma_{test} > 0$) at accelerations of 12x (top) and 16x (bottom). Supervised methods were trained with $k=1$ (solid line) or $k=14$ (dashed line) supervised scans. Shaded area (gray) indicates noise level range during training ($\mathcal{R}(\sigma_{tr})$). With only one supervised scan ($k=1$), Noise2Recon matched and exceeded performance of supervised methods trained with abundant supervised examples ($k=14$), regardless of noise augmentations and fine-tuning. Higher SSIM values indicate less blurring in Noise2Recon compared to CS and supervised DL methods. Noise2Recon image quality metrics had low sensitivity to increasing σ_{test} and acceleration, which may indicate higher robustness in noisy settings.

other hand, Supervised resulted in amplified noise artifacts in reconstructed images, which may indicate overfitting of these methods to non-noisy scans.

Additionally, supervised augmentation baselines were sensitive to the extent of training data when generalizing to different noise levels. However, Noise2Recon recovered the performance of these Supervised+Aug and Supervised+Aug-FT models trained on the full training dataset with only one supervised training scan. Additionally, while models fine-tuned from pretrained denoisers showed improved performance in noisy settings, these networks were consistently outperformed by Noise2Recon across all metrics. Noise2Recon also showed increased generalizability to noise levels outside of the range sampled during training ($\sigma_{test} \notin \mathcal{R}(\sigma_{tr})$) (Fig. 4).

Generalizing to unseen accelerations: Despite being trained on scans with a fixed acceleration factor (R_{train}), Noise2Recon generalized better to OOD accelerations ($R_{test} \neq R_{train}$) (Fig. 6). At accelerations lower than those of training scans ($R_{test} < R_{train}$), Noise2Recon reconstructions had considerably higher pSNR and SSIM than images reconstructed by supervised baselines trained

with the same number of supervised scans. As the acceleration factor increased, Noise2Recon maintained higher performance than supervised methods across all metrics. Noise2Recon performance on OOD acceleration factors also surpassed that of in-distribution generalization of supervised methods. For example, at $R_{train} = 12$ and $R_{test} = 16$, Noise2Recon outperformed supervised methods trained on $R_{train} = 16$ accelerated scans. A similar pattern was seen for $R_{train} = 16$ and $R_{test} = 12$.

5.2. Ablation Study

In these experiments, we investigate three natural design questions that may be helpful for training Noise2Recon:

1. How should supervised and unsupervised data be sampled during training?
2. How should noise levels (σ_{tr}) for training augmentations be configured?
3. How should loss weighting be selected?

We show that Noise2Recon is not very sensitive to any of these design decisions (especially 2&3), which may reduce

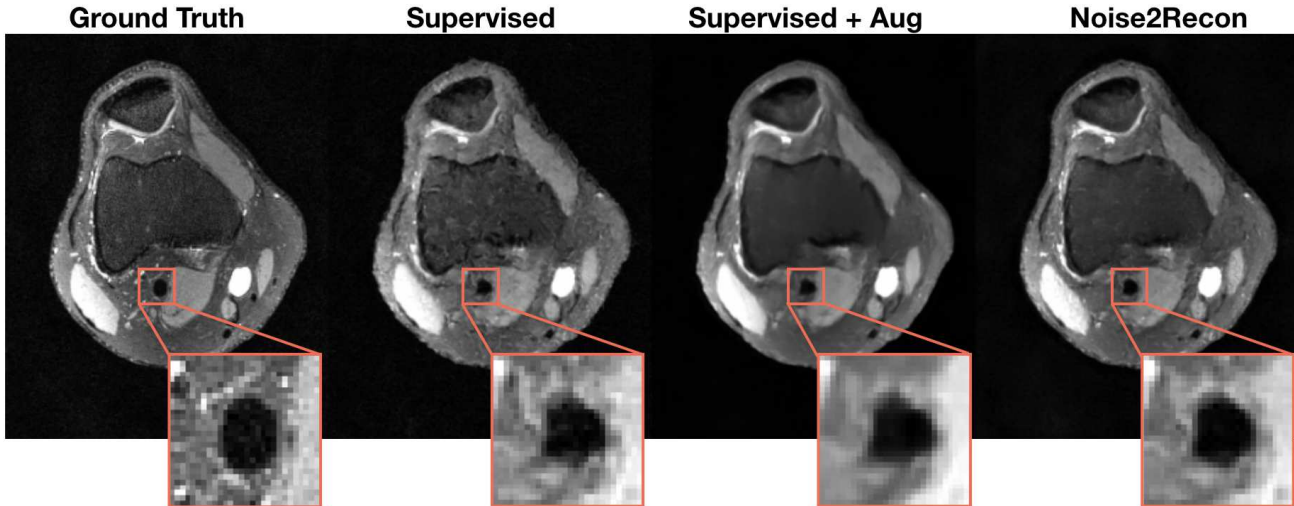


Figure 5. Sample image reconstructions for different methods in noisy settings ($\sigma=0.2$). Supervised models amplify noise artifacts, while supervised models with noise augmentations produce blurry image. Noise2Recon balances denoising and reconstruction, recovering diagnostically relevant, fine anatomical structures.

the burden of hyperparameter search during training. All ablations are performed on $k = 1$ configurations with the same hyperparameters detailed in Appendix B.

Balanced data sampling: In this ablation, we evaluated the impact of balanced sampling between supervised (S) and unsupervised (U) examples during training. Figure 8 shows the performance of balanced sampling with different $T_S:T_U$ ratios compared to random sampling. Regardless of the ratio, balanced sampling consistently outperforms random sampling across all metrics. Oversampling supervised scans relative the unsupervised scans ($T_S > T_U$) performed slightly better than oversampling unsupervised scans ($T_U > T_S$). The top two overall performance across all metrics were achieved with $T_S:T_U$ ratios of 2:1 and 1:1, respectively.

Sensitivity to training noise levels: Network stability and generalizability can often be impacted by the extent (or difficulty) of the augmentations used during training. In this ablation, we characterized how changing the interval of noise levels sampled for training augmentations (σ_{tr}) impact overall network performance for both fully supervised training methods (Supervised+Aug) and Noise2Recon. We consider two training techniques that may impact the overall difficulty of learning to generalize from augmentations: (1) noise ranges with larger intervals that increase variance of sampled noise augmentations at train time, and (2) noise ranges with larger upper bounds that account for a higher magnitude of noise-corruption.

Compared to Supervised+Aug, Noise2Recon generalized better to both in-distribution scans ($\sigma_{test} = 0$) and out-of-

distribution, noisier scans (larger noise intervals) regardless of the noise interval prescribed during training (Fig. 7). The performance of Supervised+Aug models also deteriorated more rapidly with increased noise, particularly among metrics emphasizing high-frequency information such as SSIM (Fig. 7E)

All Noise2Recon networks perform similarly in the in-distribution settings regardless of the size or extent of the training noise interval. In OOD noisy settings ($\sigma_{test} > 0$), all networks generalized poorly to testing noise levels that were not within the training noise interval ($\sigma_{test} \notin \sigma_{tr}$) (Fig. 7A-C). As a result, networks trained with small noise intervals (i.e. $\mathcal{R}(\sigma_{tr})$ is small) did not generalize at higher noise settings. However, this was mitigated by either increasing the upper bound of the noise range or increasing the extent of the noise range. Both techniques increased generalizability at high noise levels without sacrificing performance at low noise levels. Highest performance across all noise levels was observed with $\mathcal{R}(\sigma_{tr})=[0.05,1.0]$.

Sensitivity to loss weighting: In this ablation, we investigated the impact of the consistency loss weighting parameter λ on overall performance of Noise2Recon models. In the in-distribution evaluation setting, the weighting factor had negligible impact on performance between $\lambda \in [0.05, 0.8]$ (Fig. 9). At very low ($\lambda \leq 0.01$) or high ($\lambda \geq 0.8$) weighting factors, metrics reduced slightly, but within the error range. Among simulated noisy acquisitions, Noise2Recon reconstruction performance for $\lambda \in [0.05, 0.8]$ was also similar for all testing noise levels ($\sigma_{test} \in \{0, 0.1, \dots, 1\}$).

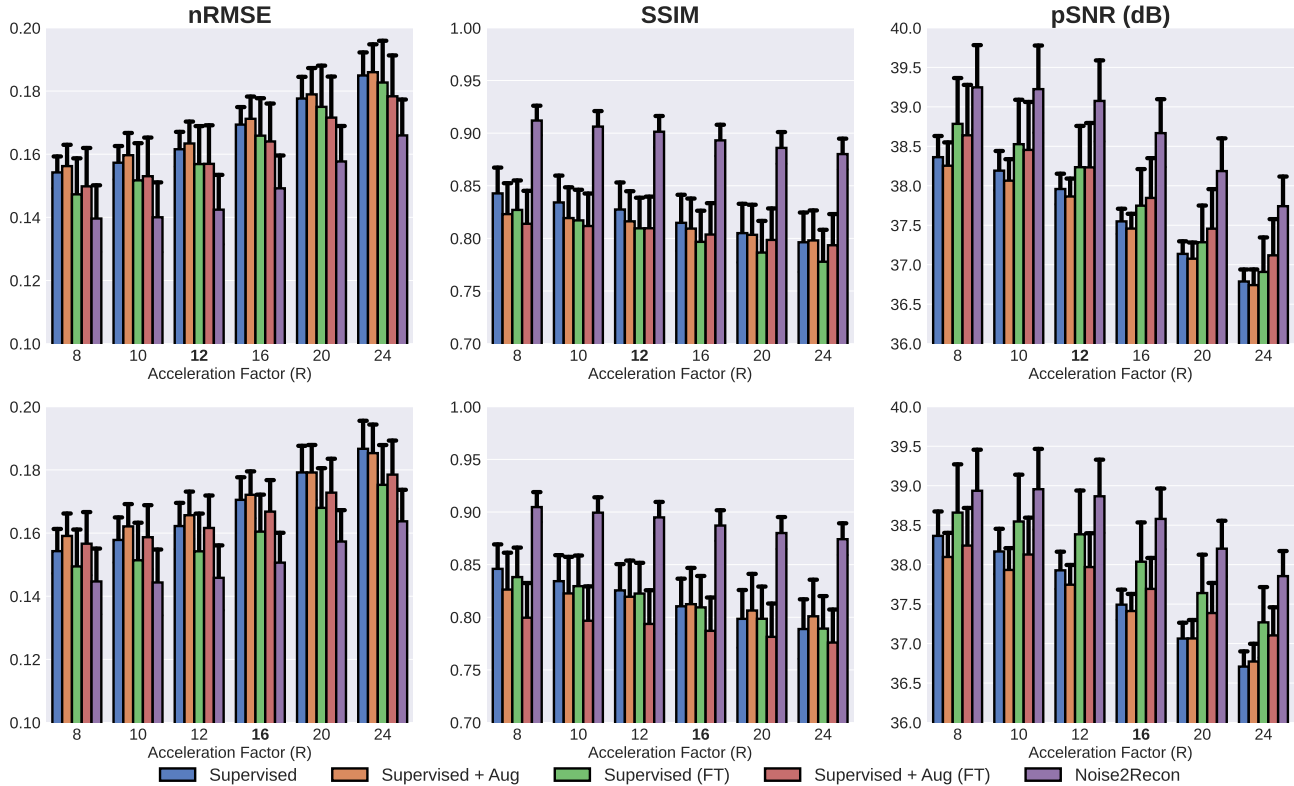


Figure 6. Generalizability of methods trained on one acceleration (bolded on x-axis) to unseen accelerations. Methods were trained on scans accelerated at $R_{train}=12$ (top row) and $R_{train}=16$ (bottom row). Noise2Recon recovers images better at both lower ($R_{test} < R_{train}$) and higher acceleration factors ($R_{test} > R_{train}$) compared to supervised methods trained on the same number of supervised scans ($k = 1$).

6. Discussion

In this work, we evaluate the efficacy of a semi-supervised framework for joint MRI reconstruction and denoising. We show that augmentation-based consistency is a viable method for recovering performance in label-scarce and OOD settings compared to both CS and supervised DL methods. In this section, we first explore the relationship between our method and principles in both compressed sensing and multi-task learning. We then discuss the practical utility of our method in data-limited and OOD settings. Finally, we detail characteristics of our method that can improve network optimization and simplify training.

Compressed sensing and denoising: In CS, recovering images from undersampled measurements is made possible by introducing incoherence through random undersampling, where resulting aliasing artifacts resemble additive Gaussian noise (Lustig et al., 2008). As a result, image recovery with CS can be viewed as a denoising problem. Noise2Recon aims to utilize the similarity between the reconstruction and denoising tasks by jointly optimizing a reconstruction and denoising objective. We observe optimizing similar tasks

jointly helps, where performance improves both in the reconstruction task (Fig. 6), and in the denoising task (Fig. 4). Our observations comply with multi-task learning theory, where given sufficient data samples and similar tasks, optimizing a multi-task objective leads to positive transfer (Wu et al., 2020). Positive transfer refers to improving performance on a task by training a joint objective of multiple tasks, compared to training a task individually.

Task-based regularization: Our joint reconstruction and denoising paradigm is reminiscent of model regularization techniques. Traditionally, these methods arise designed to reduce the variance of the model by convex constraints such that the model parameters are sparse or low-magnitude (Larsen & Hansen, 1994; Van Laarhoven, 2017). The addition of the denoising objective may not regularize the network at the parameter-level, but rather at the more semantic task-level. With the consistency objective, the regularizer is explicitly data-driven, which may help learn non-convex regularization processes that are optimal for the collected data.

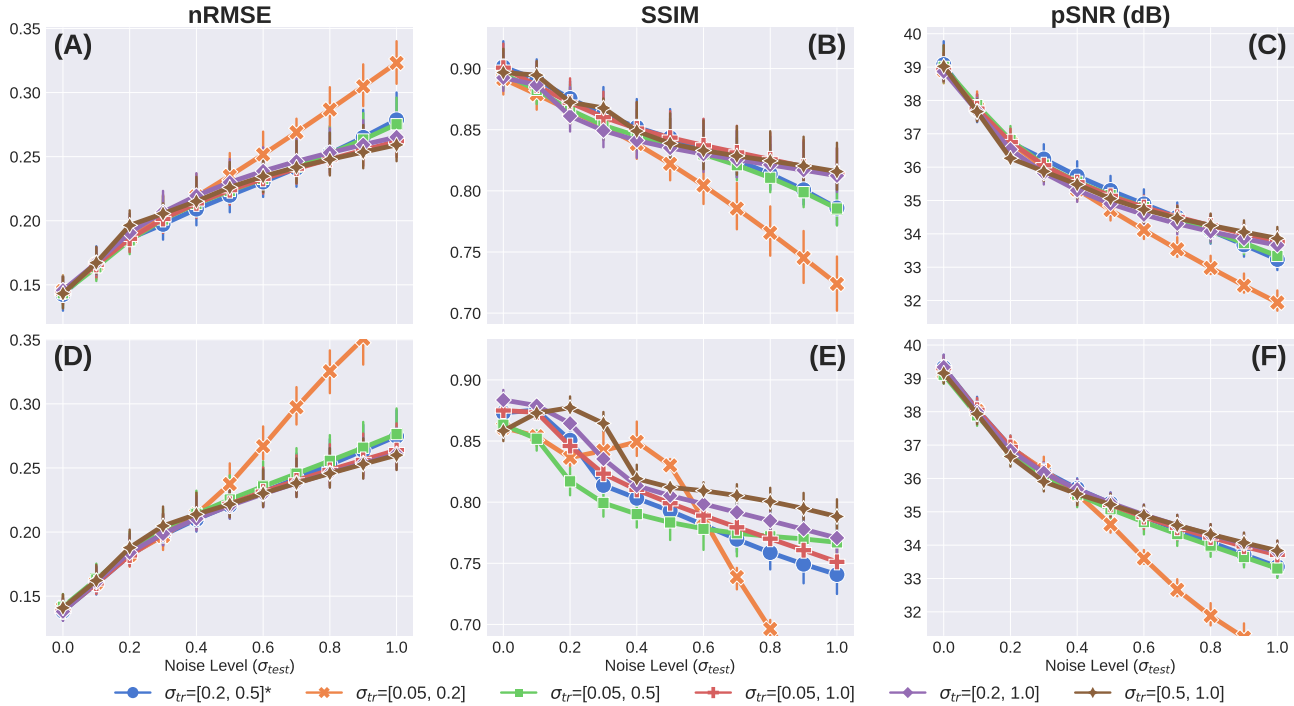


Figure 7. Impact of training noise level σ_{tr} among Noise2Recon trained with 1 supervised scan (A-C) and supervised models trained with 14 supervised scans (D-F). Performance is measured at multiple testing noise levels. Asterisk (*) indicates the default training noise level range for experiments. Noise2Recon is less sensitive to changes in σ_{tr} compared to supervised methods with noise augmentations. Higher SSIM in Noise2Recon were consistent with considerably less blurring compared to supervised methods.

Learning in label-scarce settings: Model performance is primarily dictated by the size and quality of the training data and labels (Hestness et al., 2017; Ratner et al., 2016). As a result, standard supervised methods often fail in data-limited regimes. The semi-supervised setup in Noise2Recon enables joint usage of supervised data and unsupervised data to both complement the image reconstruction task while building robustness to reconstruction of noisy scans. The increased performance of Noise2Recon over supervised baselines among in-distribution scans may indicate that the consistency framework can (1) improve the estimation of the true data distribution with more training examples and (2) generate high quality pseudo-labels that can function as noisy surrogates for the true labels without impairing training from supervised examples.

Robustness to noise: Differences in the SNR among MR acquisitions are pervasive given the heterogeneity of MR hardware (e.g. field strength, coil geometry) and sequence parameters (e.g. echo time). Reconstruction methods that can generalize better to such distribution shift may have practical utility for prospective deployment. For reconstructing noisy scans, supervised training methods benefited considerably from augmentations to training data. However, in cases of limited data, supervised methods still had con-

siderably worse performance compared to settings where supervised data is abundant. In comparison, with only 1 supervised training example ($k = 1$), Noise2Recon matched and, among some metrics, exceeded the performance of data-abundant supervised models ($k = 14$) without impairing performance on in-distribution, high SNR ($\sigma_{test} = 0$) examples. Noise2Recon achieved higher SSIM and similar pSNR and nRMSE metrics compared to even data-abundant supervised models across all testing noise levels, which may indicate that Noise2Recon minimizes global error (i.e. mean squared error) and recovers fine anatomical structure. This was also verified with visual inspection, where scans reconstructed using augmentation-based supervised methods have considerable blurring (Fig. 5). Thus, Noise2Recon (1) demonstrates utility for data-efficiency in distribution shift settings and (2) can generalize better to acquisitions at different noise levels, even compared to supervised methods with ample training data, without collapsing towards the trivial denoising solution (i.e. blurring).

Generalization under unseen distribution shift: It is intractable to capture the exhaustive set of acquisition settings in which the model should perform well. As such, it is practically useful for a deep-learning technique to be able to generalize to perturbations that were not sim-

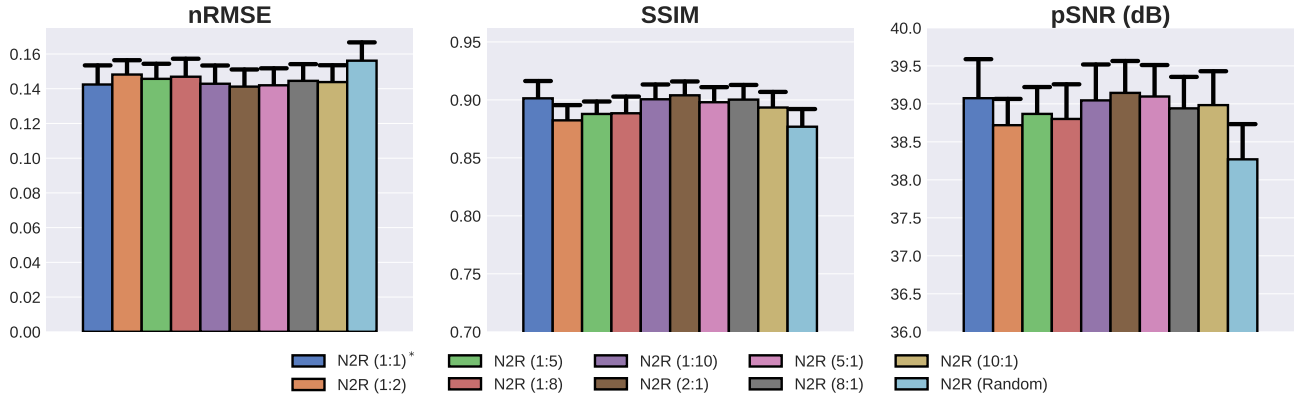


Figure 8. Balanced sampling of supervised to unsupervised scans compared to random sampling. Asterisk (*) indicates the default sampling configuration for Noise2Recon experiments. Balanced sampling, regardless of the ratio of supervised:unsupervised examples, increases average performance over standard random sampling.

ulated during training (i.e. *unseen* settings), such as unseen noise levels ($\sigma_{test} \notin \mathcal{R}(\sigma_{tr})$) and unseen accelerations ($R_{test} \neq R_{train}$). Compared to supervised methods, Noise2Recon had minimal and smoother performance loss across all σ_{test} , including unseen noise levels (Fig. 4), and recovered performance better at acceleration levels both higher and lower than those observed during training (Fig. 6). Although Noise2Recon was not explicitly trained with data simulated at different accelerations, the improved performance in these settings may suggest that the joint optimization of the reconstruction and denoising objectives contributes to positive transfer between the tasks. This observation may empirically validate that even among DL methods, noise is a reasonable model for signal incoherence, as is proposed in CS theory. Thus, learning to denoise images can also help improve reconstruction efficacy in cases where aliasing is extensive (i.e. higher accelerations). Overall, Noise2Recon may be more stable in response to larger extents of distribution shift than supervised DL methods and may be a more viable candidate for deployment in different acquisition settings.

Stabilizing multi-objective optimization: As mentioned in §3.4, magnitude of the supervised and consistency objectives are implicitly weighted by the number of supervised and unsupervised examples. Thus, random data sampling can lead to sub-optimal convergence for both objectives. Balanced sampling eliminates this weighting factor by controlling the duty cycle of supervised and unsupervised examples during optimization. We find that this sampling procedure can improve overall performance. This technique is also reminiscent of sub-group sampling in methods in distributionally robust optimization for classification models, where examples of classes are sampled at a rate inversely proportional to the class

frequency (Sagawa et al., 2019).

Insensitivity to hyperparameter selection: Multi-objective training frameworks and augmentation optimization often require careful tuning for hyperparameters due to optimization instabilities introduced with different simulated data distributions or weighted objectives. However, Noise2Recon showed minimal sensitivity to hyperparameter selection, specifically the training noise range $\mathcal{R}(\sigma_{tr})$ and the consistency loss weighting λ . Training noise ranges in Noise2Recon could be increased without degrading performance across any noise levels. This robustness is uncharacteristic of supervised approaches, which are often sensitive to augmentation intensity (Fig. 7D-F). Additionally, Noise2Recon was generally insensitive to a wide range of weighting parameters λ , which most multi-objective methods generally have to tune for superior performance. This may suggest that the consistency framework in Noise2Recon can minimize instabilities in network optimization caused by small changes in hyperparameters. This robustness to changes in hyperparameter configuration may be practically useful for simplifying network training.

Limitations and Future Work Noise2Recon is applicable in regimes where a small supervised dataset is available in conjunction with a large unsupervised dataset. However, in clinical applications such as dynamic contrast enhancement (DCE) imaging, or blood flow imaging, access to fully-sampled datasets might be impossible. In such applications where solely an unsupervised dataset is available, a supervised training objective as in Noise2Recon would not be possible, requiring a modification to the Noise2Recon training objective to incorporate an unsupervised reconstruction objective, which can be investigated in future work. We limited the scope of this study to consider noise augmen-

tations. The consistency regularization paradigm used in Noise2Recon might be extended to other artifacts observed in MRI such as motion, phase wrapping, eddy currents along with many others.

7. Conclusion

In this work, we propose Noise2Recon, a semi-supervised consistency-based framework for joint MRI reconstruction and denoising. We observe that Noise2Recon can outperform standard supervised methods in both in-distribution, high-SNR and OOD, low-SNR settings with limited training data. In addition, we show that balanced data sampling approaches can improve network optimization and reduce dependence on hyperparameters for the multi-task supervised and consistency objectives. By reducing dependence on supervised data for model training and increasing generalizability to different noise levels, Noise2Recon shows potential for reducing the burden of model retraining or fine-tuning in both research and clinical settings.

8. Acknowledgements

This work was supported by R01 AR063643, R01 EB002524, R01 EB009690, R01 EB026136, K24 AR062068, and P41 EB015891 from the NIH; the Precision Health and Integrated Diagnostics Seed Grant from Stanford University; DOD – National Science and Engineering Graduate Fellowship (ARO); National Science Foundation (GRFP-DGE 1656518, CCF1763315, CCF1563078); Stanford Artificial Intelligence in Medicine and Imaging GCP grant; Stanford Human-Centered Artificial Intelligence GCP grant; GE Healthcare and Philips.

References

- Adler, J. and Öktem, O. Learned primal-dual reconstruction. *IEEE transactions on medical imaging*, 37(6):1322–1332, 2018.
- Aggarwal, H. K., Mani, M. P., and Jacob, M. Modl: Model-based deep learning architecture for inverse problems. *IEEE Transactions on Medical Imaging*, 38(2):394–405, Feb 2019. ISSN 0278-0062, 1558-254X. doi: 10.1109/TMI.2018.2865356.
- Batson, J. and Royer, L. Noise2self: Blind denoising by self-supervision, 2019.
- Chaudhari, A. S., Sandino, C. M., Cole, E. K., Larson, D. B., Gold, G. E., Vasanaawala, S. S., Lungren, M. P., Hargreaves, B. A., and Langlotz, C. P. Prospective deployment of deep learning in mri: A framework for important considerations, challenges, and recommendations for best practices. *Journal of Magnetic Resonance Imaging*, 54(2):357–371, Aug 2021. ISSN 1053-1807, 1522-2586. doi: 10.1002/jmri.27331.
- Cole, E. K., Pauly, J. M., Vasanaawala, S. S., and Ong, F. Unsupervised mri reconstruction with generative adversarial networks, 2020.
- Darestani, M. Z. and Heckel, R. Accelerated mri with un-trained neural networks, 2021.
- Darestani, M. Z., Chaudhari, A. S., and Heckel, R. Measuring robustness in deep learning based compressive sensing. In Meila, M. and Zhang, T. (eds.), *Proceedings of the 38th International Conference on Machine Learning*, volume 139 of *Proceedings of Machine Learning Research*, pp. 2433–2444. PMLR, 18–24 Jul 2021. URL <http://proceedings.mlr.press/v139/darestani21a.html>.
- Donoho, D. L., Maleki, A., and Montanari, A. The noise-sensitivity phase transition in compressed sensing. *IEEE Transactions on Information Theory*, 57(10):6920–6941, Oct 2011. ISSN 0018-9448, 1557-9654. doi: 10.1109/TIT.2011.2165823.
- Fabian, Z., Heckel, R., and Soltanolkotabi, M. Data augmentation for deep learning based accelerated mri reconstruction with limited data. In *International Conference on Machine Learning*, pp. 3057–3067. PMLR, 2021.
- Hammernik, K., Klatzer, T., Kobler, E., Recht, M. P., Sodickson, D. K., Pock, T., and Knoll, F. Learning a variational network for reconstruction of accelerated mri data. *Magnetic resonance in medicine*, 79(6):3055–3071, 2018.
- Hendriksen, A. A., Pelt, D. M., and Batenburg, K. J. Noise2inverse: Self-supervised deep convolutional denoising for linear inverse problems in imaging, 2020.
- Hestness, J., Narang, S., Ardalani, N., Diamos, G., Jun, H., Kianinejad, H., Patwary, M., Ali, M., Yang, Y., and Zhou, Y. Deep learning scaling is predictable, empirically. *arXiv preprint arXiv:1712.00409*, 2017.
- Hu, B. S.-C. and Cheng, J. Y. System and method for noise-based training of a prediction model, May 4 2021. US Patent 10,997,501.
- Jin, K. H., McCann, M. T., Froustey, E., and Unser, M. Deep convolutional neural network for inverse problems in imaging. *IEEE Transactions on Image Processing*, 26(9):4509–4522, 2017.
- Knoll, F., Hammernik, K., Kobler, E., Pock, T., Recht, M. P., and Sodickson, D. K. Assessment of the generalization of learned image reconstruction and the potential for transfer learning. *Magnetic Resonance in Medicine*, 81(1):116–128, Jan 2019. ISSN 07403194. doi: 10.1002/mrm.27355.
- Lahiri, A., Wang, G., Ravishankar, S., and Fessler, J. A. Blind primed supervised (blips) learning for mr image reconstruction. *IEEE Transactions on Medical Imaging*, pp. 1–1, 2021. ISSN 0278-0062, 1558-254X. doi: 10.1109/TMI.2021.3093770.
- Larsen, J. and Hansen, L. K. Generalization performance of regularized neural network models. In *Proceedings of IEEE Workshop on Neural Networks for Signal Processing*, pp. 42–51. IEEE, 1994.
- Lehtinen, J., Munkberg, J., Hasselgren, J., Laine, S., Karras, T., Aittala, M., and Aila, T. Noise2noise: Learning image restoration without clean data, 2018.
- Lei, K., Mardani, M., Pauly, J. M., and Vasanaawala, S. S. Wasserstein gans for mr imaging: From paired to unpaired training. *IEEE Transactions on Medical Imaging*, 40(1):105–115, Jan 2021. ISSN 0278-0062, 1558-254X. doi: 10.1109/TMI.2020.3022968.

- Liu, J., Sun, Y., Eldeniz, C., Gan, W., An, H., and Kamilov, U. S. Rare: Image reconstruction using deep priors learned without groundtruth. *IEEE Journal of Selected Topics in Signal Processing*, 14(6):1088–1099, Oct 2020. ISSN 1932-4553, 1941-0484. doi: 10.1109/JSTSP.2020.2998402.
- Lustig, M., Donoho, D., and Pauly, J. M. Sparse mri: The application of compressed sensing for rapid mr imaging. *Magnetic Resonance in Medicine*, 58(6):1182–1195, Dec 2007. ISSN 07403194, 15222594. doi: 10.1002/mrm.21391.
- Lustig, M., Donoho, D. L., Santos, J. M., and Pauly, J. M. Compressed sensing mri. *IEEE Signal Processing Magazine*, 25(2): 72–82, 2008. doi: 10.1109/MSP.2007.914728.
- Macovski, A. Noise in mri. *Magnetic resonance in medicine*, 36(3):494–497, 1996.
- Meinhardt, T., Moeller, M., Hazirbas, C., and Cremers, D. Learning proximal operators: Using denoising networks for regularizing inverse imaging problems. In *2017 IEEE International Conference on Computer Vision (ICCV)*, pp. 1799–1808. IEEE, Oct 2017. ISBN 9781538610329. doi: 10.1109/ICCV.2017.198. URL <http://ieeexplore.ieee.org/document/8237460/>.
- Muckley, M. J., Riemenschneider, B., Radmanesh, A., Kim, S., Jeong, G., Ko, J., Jun, Y., Shin, H., Hwang, D., Mostapha, M., et al. State-of-the-art machine learning mri reconstruction in 2020: Results of the second fastmri challenge. *arXiv preprint arXiv:2012.06318*, 2020.
- Ong, F. and Lustig, M. Sigpy: a python package for high performance iterative reconstruction. In *Proceedings of the ISMRM 27th Annual Meeting, Montreal, Quebec, Canada*, volume 4819, 2019.
- Ong, F., Amin, S., Vasanawala, S., and Lustig, M. Mridata. org: An open archive for sharing mri raw data. In *Proc. Intl. Soc. Mag. Reson. Med*, volume 26, 2018.
- Pezzotti, N., Yousefi, S., Elmahdy, M. S., van Gemert, J., Schülke, C., Doneva, M., Nielsen, T., Kastruyulin, S., Lelieveldt, B. P. F., van Osch, M. J. P., de Weerd, E., and Staring, M. An adaptive intelligence algorithm for undersampled knee mri reconstruction: Application to the 2019 fastmri challenge, 2020.
- Pruessmann, K. P., Weiger, M., Scheidegger, M. B., and Boesiger, P. Sense: Sensitivity encoding for fast mri. *Magnetic Resonance in Medicine*, 42(5):952–962, 1999. doi: [https://doi.org/10.1002/\(SICI\)1522-2594\(199911\)42:5\(952::AID-MRM16\)3.0.CO;2-S](https://doi.org/10.1002/(SICI)1522-2594(199911)42:5(952::AID-MRM16)3.0.CO;2-S). URL <https://onlinelibrary.wiley.com/doi/abs/10.1002/%28SICI%291522-2594%28199911%2942%3A5%3C952%3A%3AAID-MRM16%3E3.0.CO%3B2-S>.
- Ratner, A. J., De Sa, C. M., Wu, S., Selsam, D., and Ré, C. Data programming: Creating large training sets, quickly. *Advances in neural information processing systems*, 29:3567–3575, 2016.
- Romano, Y., Elad, M., and Milanfar, P. The little engine that could: Regularization by denoising (red). *SIAM Journal on Imaging Sciences*, 10(4):1804–1844, 2017.
- Ronneberger, O., Fischer, P., and Brox, T. U-net: Convolutional networks for biomedical image segmentation. In *International Conference on Medical image computing and computer-assisted intervention*, pp. 234–241. Springer, 2015.
- Sagawa, S., Koh, P. W., Hashimoto, T. B., and Liang, P. Distributionally robust neural networks. In *International Conference on Learning Representations*, 2019.
- Sandino, C. M., Cheng, J. Y., Chen, F., Mardani, M., Pauly, J. M., and Vasanawala, S. S. Compressed sensing: From research to clinical practice with deep neural networks: Shortening scan times for magnetic resonance imaging. *IEEE Signal Processing Magazine*, 37(1):117–127, 2020.
- Sohn, K., Berthelot, D., Li, C.-L., Zhang, Z., Carlini, N., Cubuk, E. D., Kurakin, A., Zhang, H., and Raffel, C. Fixmatch: Simplifying semi-supervised learning with consistency and confidence, 2020.
- Soltanayev, S. and Chun, S. Y. Training deep learning based denoisers without ground truth data, 2021.
- Van Laarhoven, T. L2 regularization versus batch and weight normalization. *arXiv preprint arXiv:1706.05350*, 2017.
- Venkatakrishnan, S. V., Bouman, C. A., and Wohlberg, B. Plug-and-play priors for model based reconstruction. In *2013 IEEE Global Conference on Signal and Information Processing*, pp. 945–948, 2013. doi: 10.1109/GlobalSIP.2013.6737048.
- Virtue, P. and Lustig, M. The empirical effect of gaussian noise in undersampled mri reconstruction. *Tomography*, 3(4):211–221, Dec 2017. ISSN 2379-139X. doi: 10.18383/j.tom.2017.00019.
- Wang, Z., Bovik, A. C., Sheikh, H. R., and Simoncelli, E. P. Image quality assessment: from error visibility to structural similarity. *IEEE transactions on image processing*, 13(4):600–612, 2004.
- Wu, S., Zhang, H. R., and Ré, C. Understanding and improving information transfer in multi-task learning, 2020.
- Xie, Q., Dai, Z., Hovy, E., Luong, T., and Le, Q. Unsupervised data augmentation for consistency training. In Larochelle, H., Ranzato, M., Hadsell, R., Balcan, M. F., and Lin, H. (eds.), *Advances in Neural Information Processing Systems*, volume 33, pp. 6256–6268. Curran Associates, Inc., 2020. URL <https://proceedings.neurips.cc/paper/2020/file/44feb0096faa8326192570788b38c1d1-Paper.pdf>.
- Yaman, B., Hosseini, S. A. H., Moeller, S., Ellermann, J., Ugurbil, K., and Akcakaya, M. Self-supervised physics-based deep learning mri reconstruction without fully-sampled data. In *2020 IEEE 17th International Symposium on Biomedical Imaging (ISBI)*, pp. 921–925. IEEE, Apr 2020. ISBN 9781538693308. doi: 10.1109/ISBI45749.2020.9098514. URL <https://ieeexplore.ieee.org/document/9098514/>.
- Ying, L. and Sheng, J. Joint image reconstruction and sensitivity estimation in sense (jsense). *Magnetic Resonance in Medicine: An Official Journal of the International Society for Magnetic Resonance in Medicine*, 57(6):1196–1202, 2007.
- Zhang, K., Zuo, W., Chen, Y., Meng, D., and Zhang, L. Beyond a gaussian denoiser: Residual learning of deep cnn for image denoising. *IEEE Transactions on Image Processing*, 26(7): 3142–3155, 2017.
- Zhao, H., Gallo, O., Frosio, I., and Kautz, J. Loss functions for image restoration with neural networks. *IEEE Transactions on computational imaging*, 3(1):47–57, 2016.

A. Implementation Details

This section describes method implementations for different configurations of Noise2Recon and baselines.

A.1. Network Architecture

The U-Net architecture used in our experiments had 4 pooling layers, where the first convolution in the model had 32 output channels. Each resolution of the U-Net consisted of a convolutional block with two 3×3 convolutions followed by instance normalization and a leaky Rectified Linear Unit (ReLU) with slope $\alpha=0.2$.

A.2. Pretrained Denoisers & Fine-Tuning

Prior work has shown promise for denoisers being used for general families of inverse problems (Romano et al., 2017; Lehtinen et al., 2018). To investigate the efficacy of using denoising networks as a basis for MRI reconstruction, we considered pretraining denoising networks. These networks were subsequently fine-tuned for the MR image reconstruction task.

Denoising networks were trained following a similar protocol to the one proposed in (Batson & Royer, 2019). Because denoising can be formulated as an unsupervised problem, both fully-sampled and undersampled-only scans were used for training. To simulate a larger extent of training examples, fully-sampled scans were undersampled following the same undersampling pattern (Poisson Disc) and acceleration rate that would be used during fine-tuning. All examples were augmented with zero-mean complex-Gaussian masked noise with standard deviation σ_{tr} sampled from range $\mathcal{R}(\sigma_{tr})$. The range $\mathcal{R}(\sigma_{tr})=[0.2, 0.5)$ was chosen to be consistent with the range used for Noise2Recon and Supervised+Aug methods. The model was trained to recover the original, non-augmented image from the noise-augmented input. All denoisers were trained with the complex- ℓ_1 objective. For fine-tuning, the network was initialized with the weights resulting in the lowest validation loss and trained following the supervised protocol detailed in §4.4.

A.3. Compressed Sensing

In CS, careful tuning of the regularization parameter λ is required for each application. As the noise level σ and the acceleration factor R are varied, the sparsity level and the blurring of the input zero-filled image changes. Therefore, the regularization parameter λ was chosen based on visual tuning for various noise levels and acceleration factors independently. The optimal λ found for each setting is provided in Table 2. We observed that a high λ is needed at high noise levels σ to preserve reconstruction fidelity, whereas a lower λ is needed at lower acceleration factors R to prevent blurring. Independent of λ , CS converged at 25 iterations,

where we observed that higher number of iterations did not improve performance. In contrast to CS, Noise2Recon does not require visual tuning of its parameters, and is more robust to different noise levels at inference time.

B. Additional Experimental Results

This section provides details regarding additional experiments.

All models were trained with the following configurations unless otherwise noted. Noise2Recon models were trained with 1 supervised training subject and 13 unsupervised training subjects with 1:1 balanced sampling between supervised and unsupervised scans. Consistency loss weight was $\lambda = 0.1$. During training, the noise level was sampled at random from the specified range $\mathcal{R}(\sigma_{tr})$. Supervised+Aug models were trained with 14 supervised training subjects with 20% probability ($p=0.2$) of applying augmentations.

B.1. Scaling with Increasing Unsupervised Data

In practice, the undersampled-only (unlabeled) scans are more prevalent and collected more frequently than fully-sampled (labeled) scans. In this ablation, we explore the impact of increasing the number of undersampled examples during training. Models were trained with 1 fully-sampled scan and 2, 3, 5, or 13 undersampled scans. Noise2Recon performance improved as the number of undersampled scans used for training increased (Fig. 10). The increased performance with larger undersampled datasets may indicate that Noise2Recon is robust to size imbalances in supervised and unsupervised datasets. As the framework relies on pseudo-label generation, this observation may suggest that the quality of pseudo-labels improves with more undersampled scans.

B.2. Supervised Augmentation Probability p

In this ablation, we measure the effect of augmentation probability on supervised training with noise augmentations (Supervised+Aug). Supervised baselines were trained with noise augmentations applied with probabilities of $p=0.1, 0.2, 0.3,$ and 0.5 . Highest performance was observed at configurations $p=0.2$ and $p=0.3$ (Table 3). Augmentation probability $p=0.2$ was selected as the default configuration for training all supervised methods with noise augmentations.

B.3. Sample Reconstructions Under Real Noise

In 3D scans, SNR profile can change based on the spatial encoding of the slice. To assess the performance of Noise2Recon in reconstruction from a low-SNR image, we visualized an edge slice from the test set where the inher-

R Noise Level	0	0.2	0.4	0.6	0.8	1.0
12x	0.07	0.15	0.3	0.6	0.9	1.2
16x	0.06	0.12	0.25	0.5	0.8	1.1

Table 2. Regularization parameter selection for compressed sensing at various noise levels with 12x and 16x acceleration (R).

	SSIM	nRMSE	pSNR (dB)
Supervised+Aug ($p=0.1$)	0.875 (0.012)	0.139 (0.011)	39.3 (0.476)
Supervised+Aug ($p=0.2$)*	0.889 (0.010)	0.137 (0.011)	39.4 (0.486)
Supervised+Aug ($p=0.3$)	0.894 (0.009)	0.136 (0.010)	39.4 (0.440)
Supervised+Aug ($p=0.5$)	0.861 (0.007)	0.142 (0.009)	39.1 (0.342)

Table 3. The effect of augmentation probability p on in-distribution performance ($\sigma_{test} = 0$) of supervised baselines trained with noise augmentations (Supervised+Aug). Highest performance is achieved at $p=0.2, 0.3$. Asterisk indicates the default augmentation probability used for baseline augmentation methods.

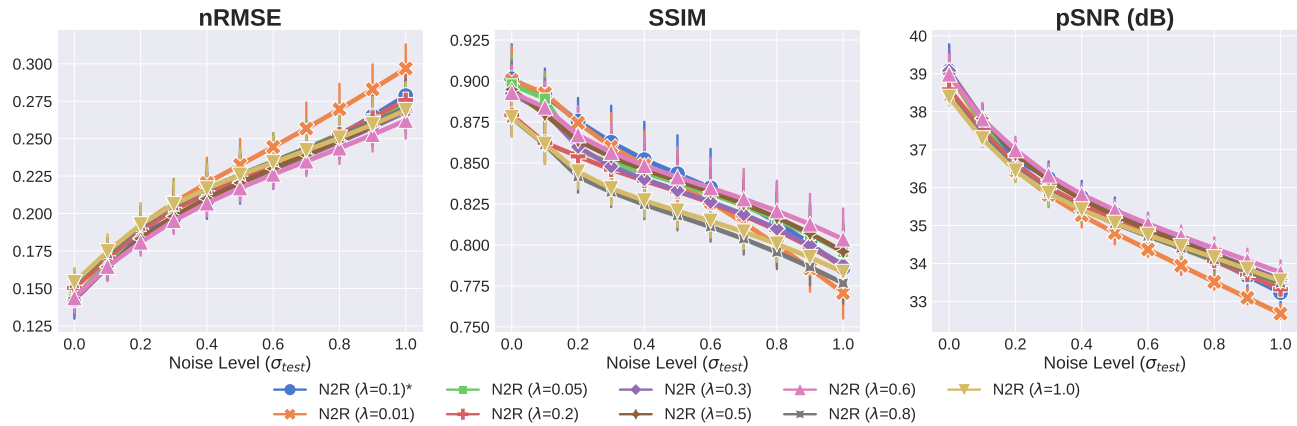


Figure 9. Impact of consistency loss weighting λ on reconstructing scans at different noise levels. Asterisk (*) indicates the default loss weighting configuration for experiments. Performance of Noise2Recon did not change for large range of $\lambda \in [0.05, 0.8]$.

ent noise observed during acquisition for the ground-truth was higher compared to middle slices. We observed that Noise2Recon can produce robust reconstructions regardless of spatially-localized SNR differences (Fig. 11).

C. Sample Zero-Filled Reconstructions of Noisy Images

In our experiments, σ_{test} was varied from 0, 0.1, ..., 1.0. On a representative test knee slice, we demonstrate the impact of noise on zero-filled, SENSE-reconstructed images at acceleration rate $R = 12$ for noise levels $\sigma_{test} \in \{0, 0.1, 0.2, 0.3, 0.4, 0.5\}$ in Fig. 12.

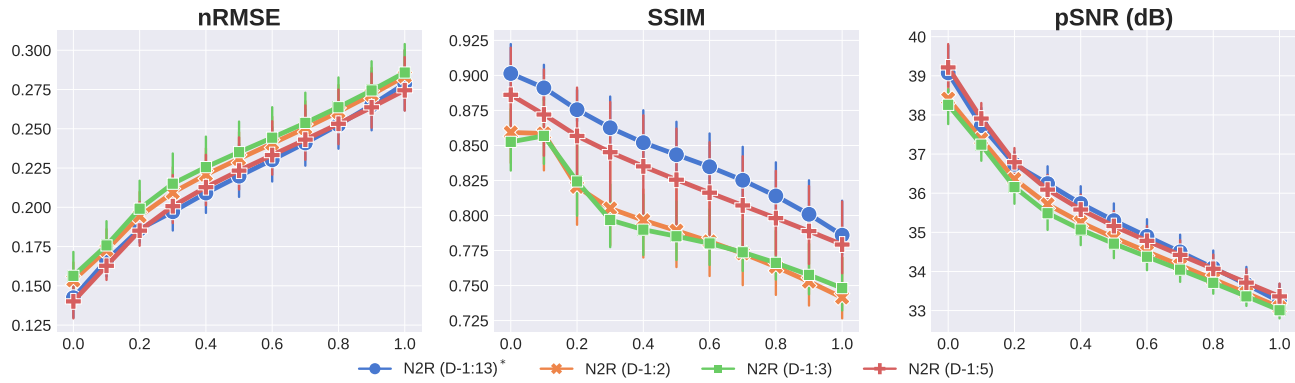


Figure 10. Noise2Recon performance with increasing number of unsupervised examples. Notation $A:B$ denotes A supervised scans and B unsupervised scans for training. Metrics are computed at multiple simulated noise levels.

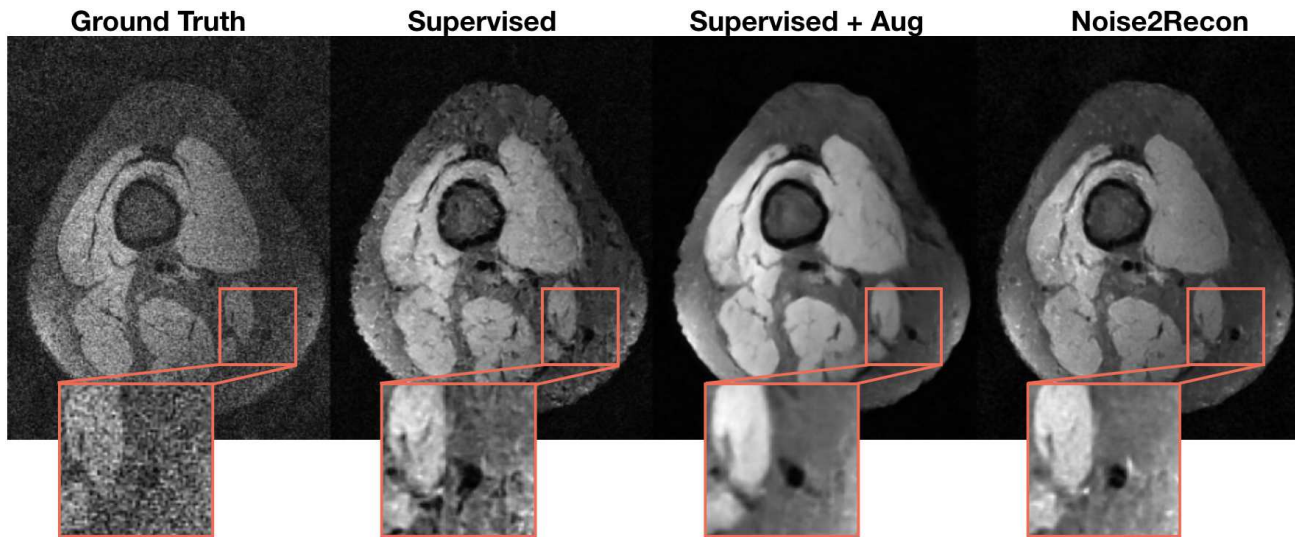


Figure 11. Sample reconstruction from an edge slice for different methods. When presented with a noisy, undersampled image at inference time, Noise2Recon jointly performs denoising and reconstruction to recover anatomies that were acquired with a low-SNR during acquisition.

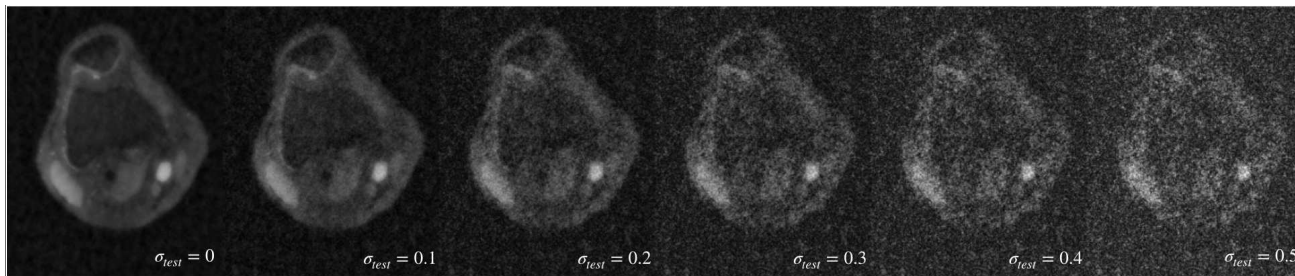


Figure 12. Zero-filled, SENSE-reconstructed images are shown at acceleration rate $R = 12$ under various noise levels $\sigma_{test} \in \{0, 0.1, 0.2, 0.3, 0.4, 0.5\}$.